Hexagonal Ti_2B_2 monolayer: A Promising Anode Material Offering High Rate Capability for Li-Ion and Na-Ion Batteries

Tao Bo[a,b], Peng-Fei Liu[a,b], Juping Xu[a,b], Junrong Zhang[a,b], Yuanbo Chen[a,b], Olle Eriksson[c], Fangwei Wang[a,b,d], Bao-Tian Wang[a,b,*]

[a] Institute of High Energy Physics, Chinese Academy of Science (CAS), Beijing 100049, China

[b] Dongguan Neutron Science Center, Dongguan 523803, China

[c] Department of Physics and Astronomy, Division of Materials Theory, Uppsala University, Box 516, SE-75120 Uppsala, Sweden

[d] Beijing National Laboratory for Condensed Matter Physics, Institute of Physics, Chinese Academy of Sciences, Beijing 100080, China

E-mail: wangbt@ihep.ac.cn

1. Computational method

The particle-swarm optimization (PSO) scheme, as implemented in the CALYPSO code,[1-3] is employed to search for low energy 2D Ti_2B_2 structures. During the structural searches, both planar and buckled structures including one, two, and three layers are all considered. In our PSO calculations, the population size is set as 30, and the number of generation is maintained at 30. Simulating cells containing 1, 2, and 4 formula units are considered for 2D Ti_2B_2.

The underlying energy calculations and structure optimizations are performed by using the plane-wave-based density-functional theory (DFT) method as implemented in the Vienna ab-initio Simulation Package (VASP).[4-6] The Perdew-Burke-Ernzerhof form of the generalized gradient approximation (PBE-GGA)[7] is chosen to describe the exchange-correlation energy. The projector augmented wave (PAW) method[8, 9] was used to describe the electron-ion interaction. The valence electrons in pseudopotentials are $2s^12p^0$ for Li, $2s^22p^1$ for B, $3s^13p^0$ for Na, $3p^13d^14s^1$ for Sc, $3d^34s^1$ for Ti, $3d^44s^1$ for V, $3d^54s^1$ for Cr, $4s^24p^64d^15s^2$ for Y, $4s^24p^64d^25s^2$ for Zr, and $4d^55s^1$ for Mo. Spin-polarization is included in all the studied systems. The cutoff energy is set as 600 eV

and the convergence criteria of the electron self-consistent is set as 10^{-5} eV. All the geometries are optimized until the forces on the atoms are smaller than 0.01 eV $Å^{-1}$.

To calculate the lattice parameters of these bulk and 2D TMBs, unit cells with 3 atoms for the bulk TMB_2 and 4 atoms for the 2D TM_2B_2 are used and the Brillouin-zone (BZ) integration is performed using 11×11×11 and 11×11×1 *k*-point grids for the bulk and 2D structures, respectively. To simulate the adsorption and diffusion of Li and Na on the Ti_2B_2 monolayer, a 2×2 supercell is used and the BZ integration is performed using 5×5×1 *k*-point grid. A vacuum separation is set to more than 20 Å to prevent any interaction between two neighboring monolayers. The optB86b-vdW exchange functional[10] is used for the van der Waals (vdW) correction since it can properly treat the long-range dispersive interactions. The importance of this exchange functional has long been recognized in predicting ground states and describing the interlayer distance in different classes of materials.[11]

To investigate the dynamical stability of these 2D TMBs, the PHONOPY package[12] is employed to calculate the phonon dispersion curves by using the density-functional perturbation theory (DFPT).[13] The Born-Oppenheimer ab initio molecular dynamics (AIMD) simulations are employed at different temperatures up to 3000 K to investigate the thermal stability of the Ti_2B_2 monolayer and at 300 K to investigate the lithium and sodium migration dynamics on the Ti_2B_2 monolayer. The AIMD simulations are performed using a 3×3 supercell with the NVT ensemble. All the dynamic simulations last for 10 ps with time steps of 1.0 fs. The BZ integration is performed using 1×1×1 *k*-point grid during the AIMD simulations.

The climbing image nudged elastic band (CI-NEB) method[14-16] is used to investigate the diffusion paths of lithium and sodium on the Ti_2B_2 monolayer. Eight images including the initial and the final positions are used for the CI-NEB calculations. The force convergence for the optimization is set as 0.02 eV $Å^{-1}$.

2. Metastable isomers of 2D Ti_2B_2.

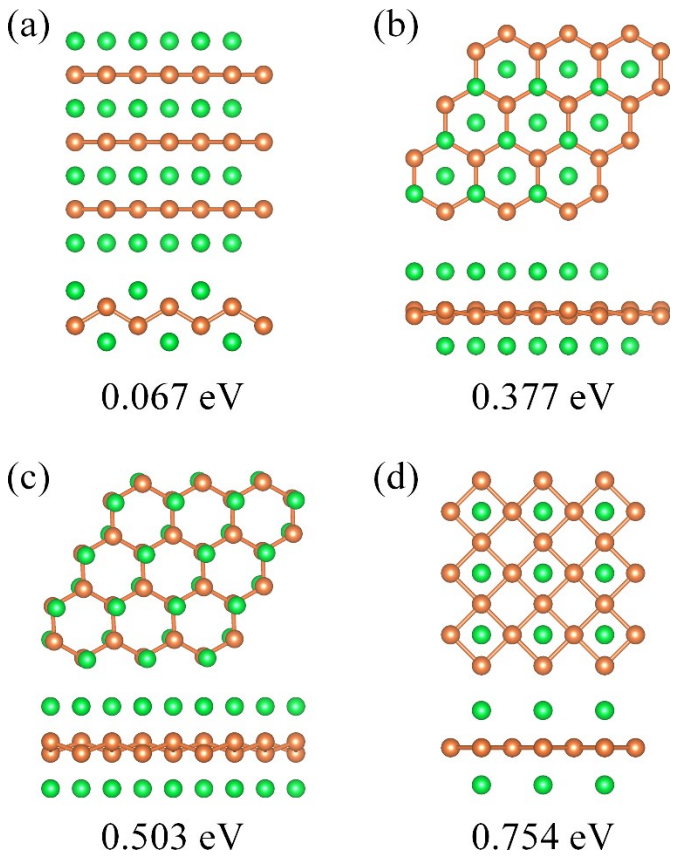

Fig. S1. Metastable isomers of 2D Ti_2B_2 found by the CALYPSO structure search. The Ti and B atoms are denoted by green and orange spheres, respectively.

3. The global minimum 2D Ti_2B_2 monolayer.

Table S1. Lattice constants (Å) of the bulk TMB_2 phases and the 2D TM_2B_2 structures. *d* represents the calculated thickness (Å) of the 2D TM_2B_2 structures.

Bulk	*a* (This)	*a* (Expt.)	*c* (This)	*c* (Expt.)	2D	*a* (This)	*d* (This)
ScB_2	3.134	3.148	3.507	3.515	Sc_2B_2	3.110	3.460
TiB_2	3.031	3.030	3.220	3.229	Ti_2B_2	3.004	3.119
VB_2	2.994	2.995	3.017	3.052	V_2B_2	2.940	2.832
CrB_2	2.954	2.973	3.025	3.072	Cr_2B_2	2.921	2.651
YB_2	3.292	3.304	3.841	3.847	Y_2B_2	3.268	3.755
ZrB_2	3.167	3.165	3.539	3.520	Zr_2B_2	3.144	3.391
MoB_2	3.017	3.005	3.352	3.173	Mo_2B_2	3.070	2.833

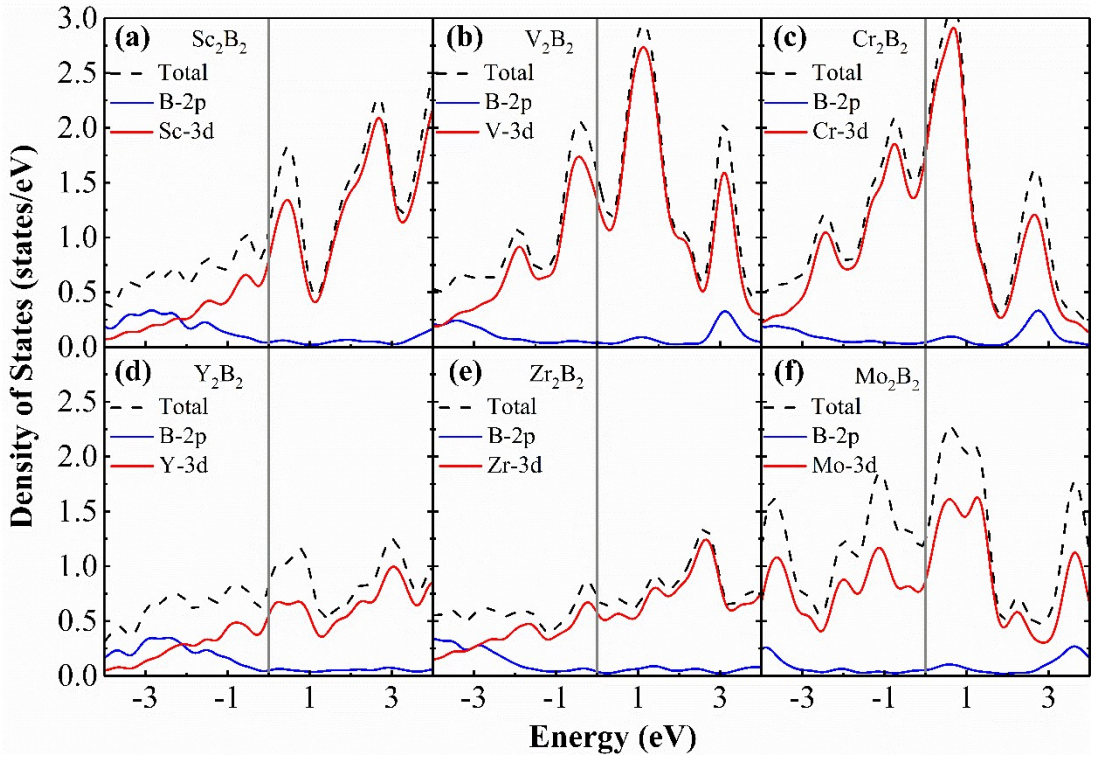

Fig. S2. Total and partial density of states of the 2D (a) Sc_2B_2, (b) V_2B_2, (c) Cr_2B_2, (d) Y_2B_2, (e) Zr_2B_2, and (f) Mo_2B_2.

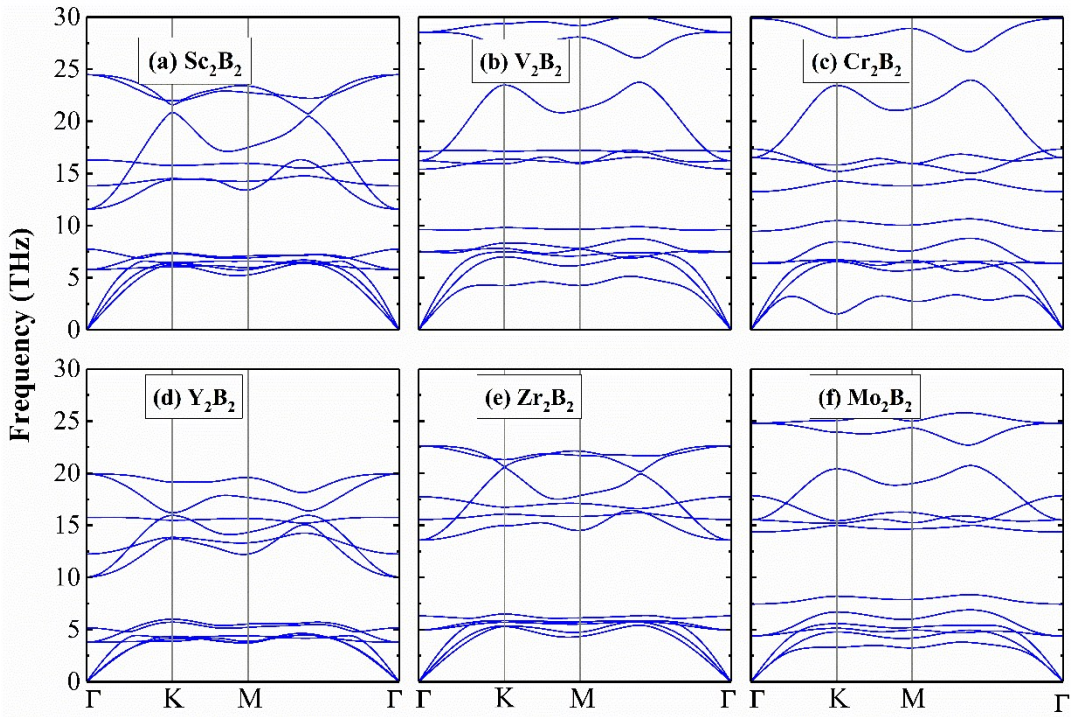

Fig. S3. Calculated phonon dispersion curves of the 2D (a) Sc_2B_2, (b) V_2B_2, (c) Cr_2B_2, (d) Y_2B_2, (e) Zr_2B_2, and (f) Mo_2B_2.

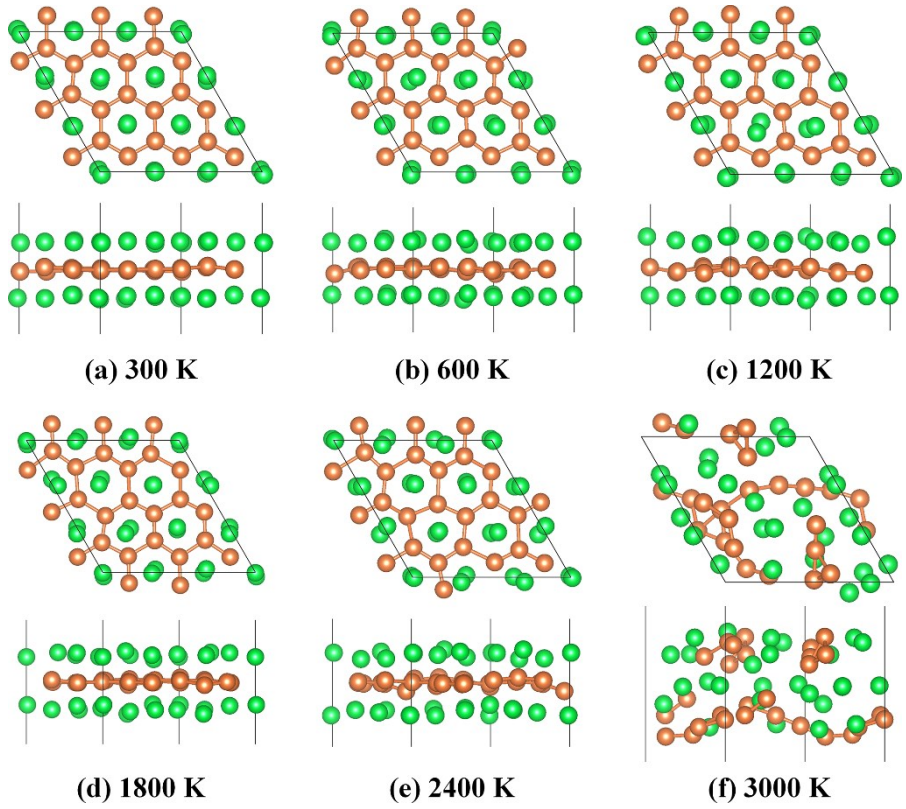

Fig. S4. Snapshots of the 2D Ti_2B_2 monolayer at temperatures from 300 to 3000 K (top and side views) at the end of 10 ps ab-initio molecular dynamics (AIMD) simulations. The Ti and B atoms are denoted by green and orange spheres, respectively.

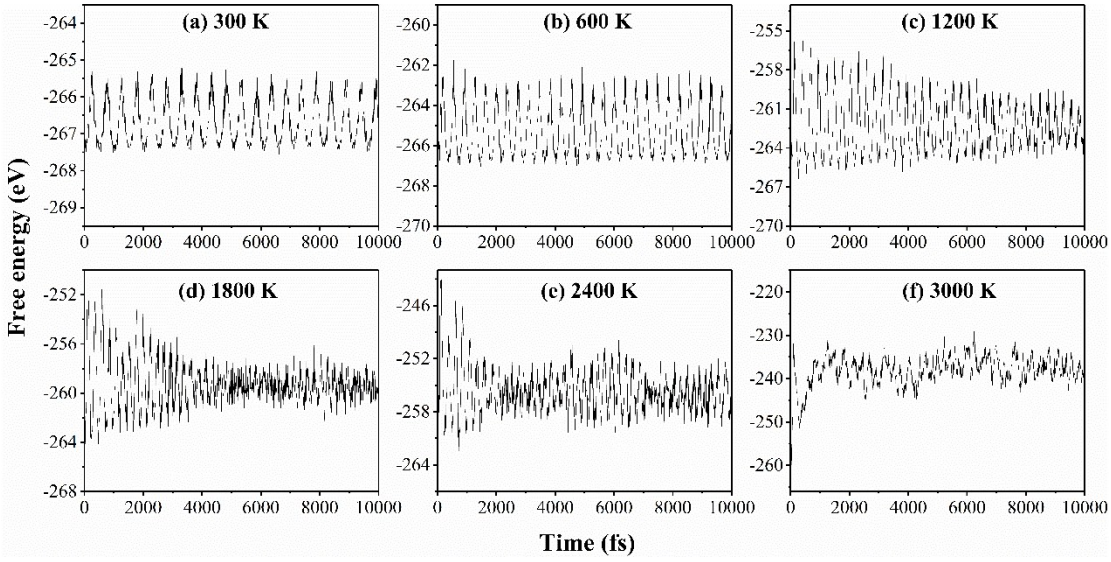

Fig. S5. Variation of the free energy in the AIMD simulations from 300 to 3000 K during the time scale of 10 ps.

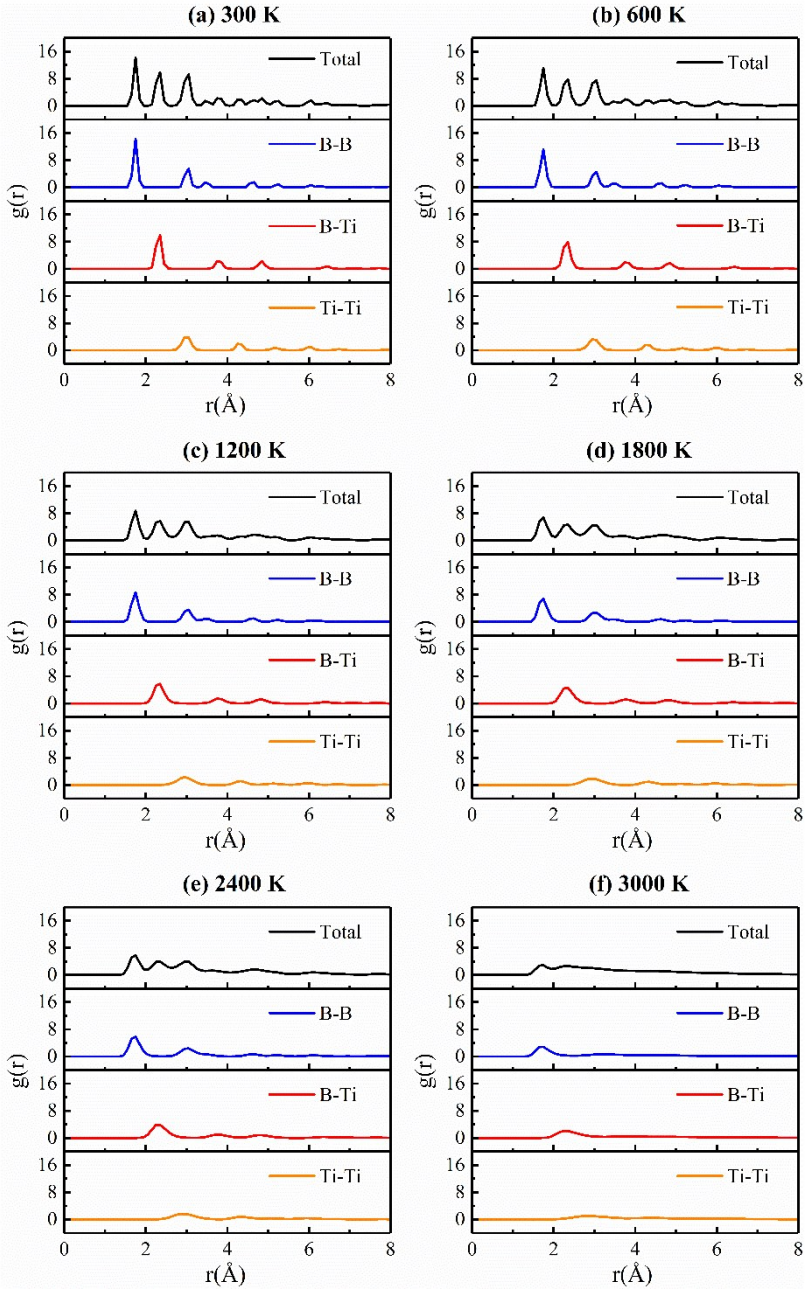

Fig. S6. Radius distribution function (RDF) for 2D Ti_2B_2 at (a) 300 K, (b) 600 K, (c) 1200 K, (d) 1800 K, (e) 2400 K, and (f) 3000 K, respectively.

4. Adsorption of Li/Na on the hexagonal Ti_2B_2 monolayer.

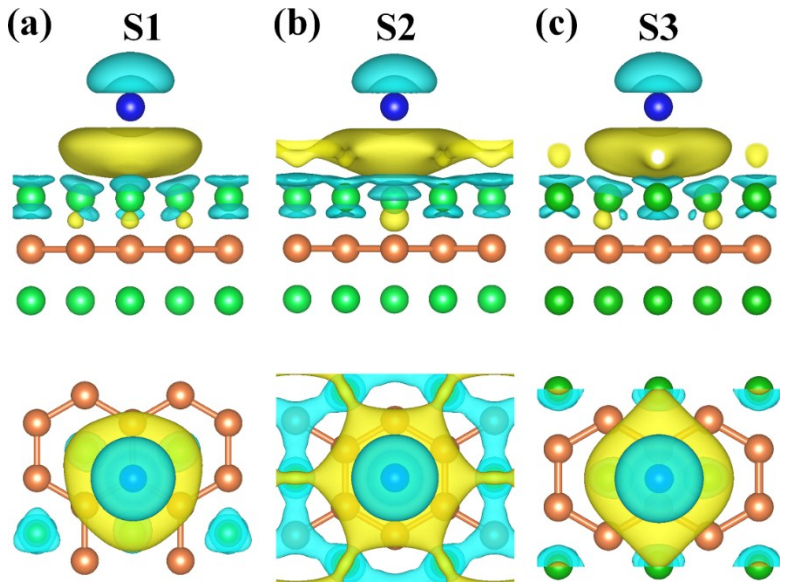

Fig. S7. The charge density difference plots for Na adsorption on the (a) S1, (b) S2, and (c) S3 sites of 2D Ti_2B_2 monolayer. The Ti, B, and Na atoms are denoted by green, orange, and blue spheres, respectively. The yellow and cyan areas represent electron gains and loses.

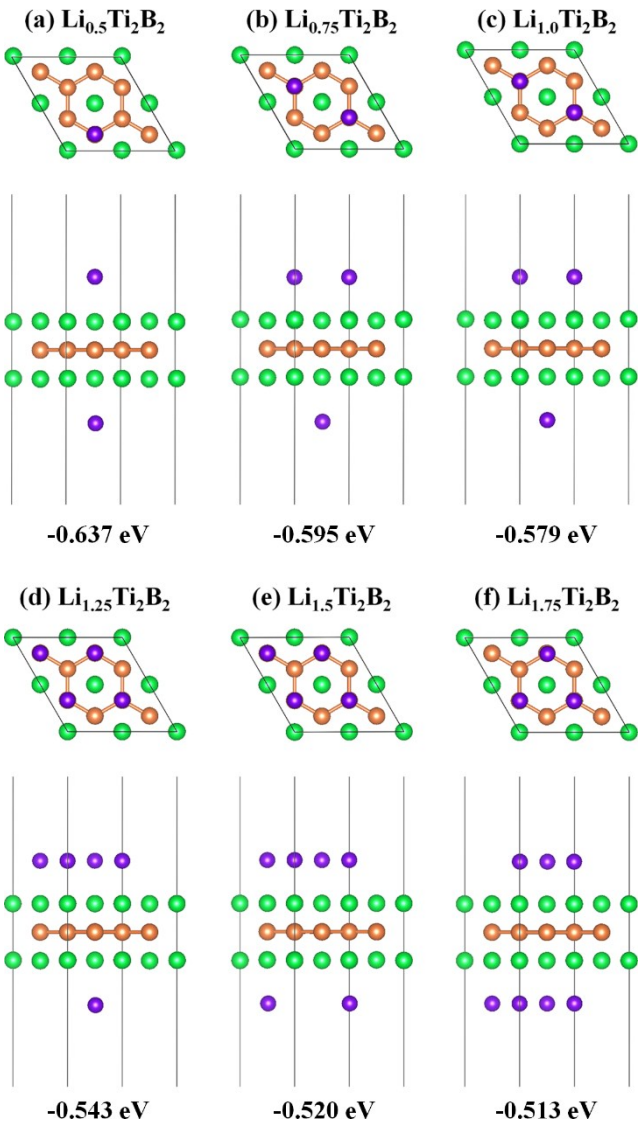

Fig. S8. Top and side views of the structures of (a) $Li_{0.5}Ti_2B_2$, (b) $Li_{0.75}Ti_2B_2$, (c) $Li_{1.0}Ti_2B_2$, (d) $Li_{1.25}Ti_2B_2$, (e) $Li_{1.5}Ti_2B_2$, and (f) $Li_{1.75}Ti_2B_2$ with Li ions adsorbed on the surface of 2D Ti_2B_2 monolayer. The Ti, B, and Li atoms are denoted by green, orange, and violet spheres, respectively.

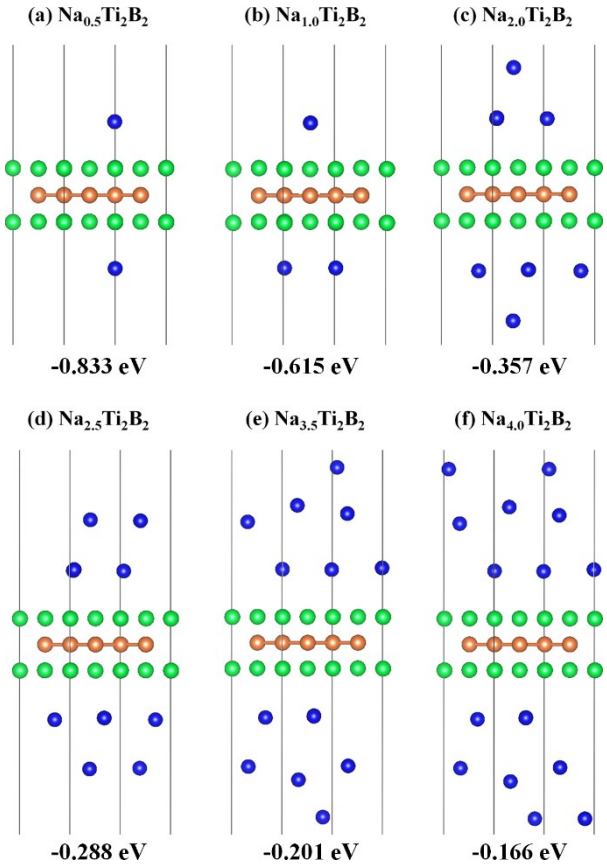

Fig. S9. Side views of the structures of (a) $Na_{0.5}Ti_2B_2$, (b) $Na_{1.0}Ti_2B_2$, (c) $Na_{2.0}Ti_2B_2$, (d) $Na_{2.5}Ti_2B_2$, (e) $Na_{3.5}Ti_2B_2$, and (f) $Na_{4.5}Ti_2B_2$ with Na ions adsorbed on the surface of 2D Ti_2B_2 monolayer. The Ti, B, and Na atoms are denoted by green, orange, and blue spheres, respectively.

5. The 2D TiB_4 structures and the adsorption and diffusion of Li/Na on the hexagonal TiB_4 monolayer.

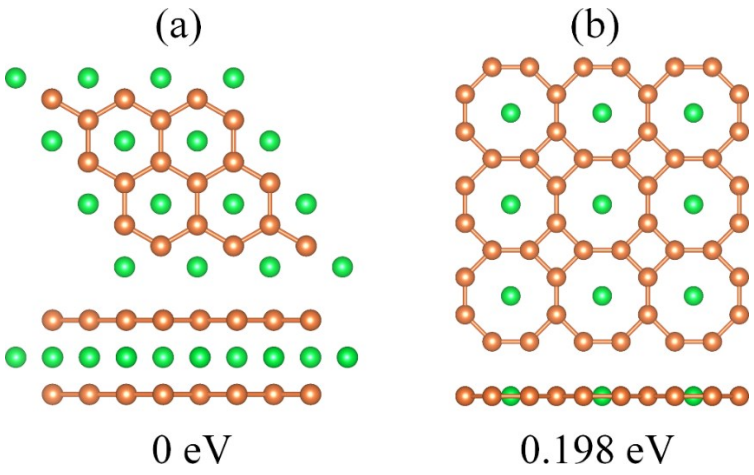

Fig. S10. (a) The hexagonal 2D TiB_4 structure. (b) The most stable planar 2D TiB_4.[17]

The Ti and B atoms are denoted by green and orange spheres, respectively.

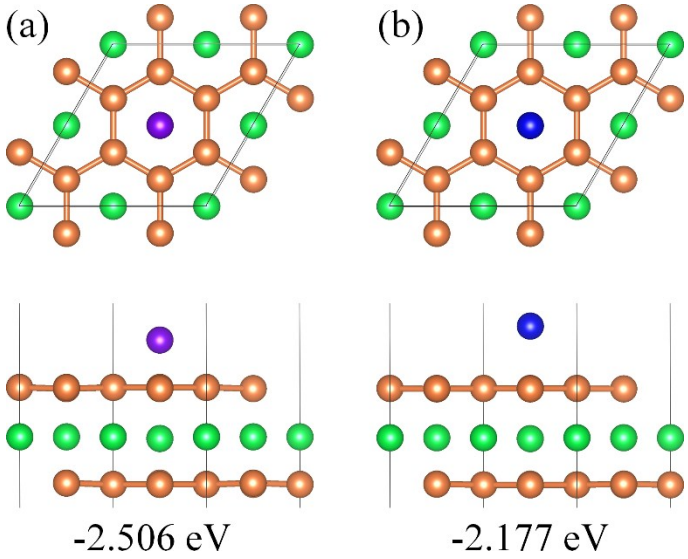

Fig. S11. Top and side views of the adsorption of (a) Li and (b) Na on the hexagonal 2D TiB_4 surface. The Ti, B, Li, and Na atoms are denoted by green, orange, violet, and blue spheres, respectively.

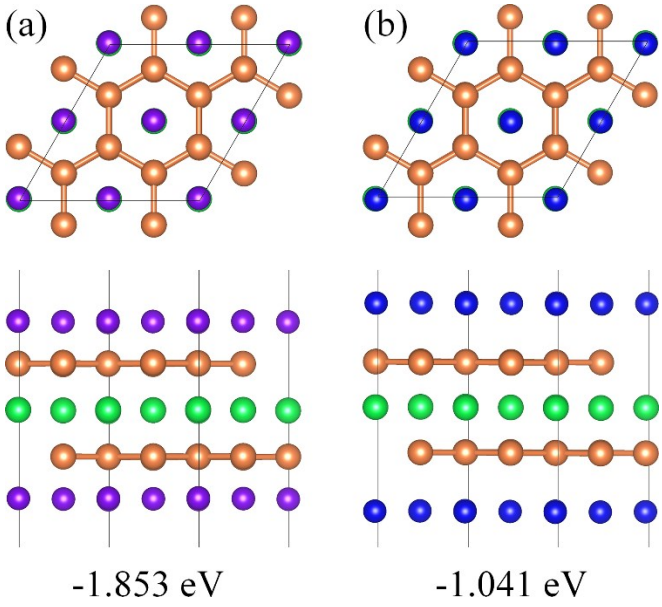

Fig. S12. Top and side views of the adsorption of (a) one-layer Li and (b) one-layer Na on the hexagonal 2D TiB_4 surface. The Ti, B, Li, and Na atoms are denoted by green, orange, violet, and blue spheres, respectively.

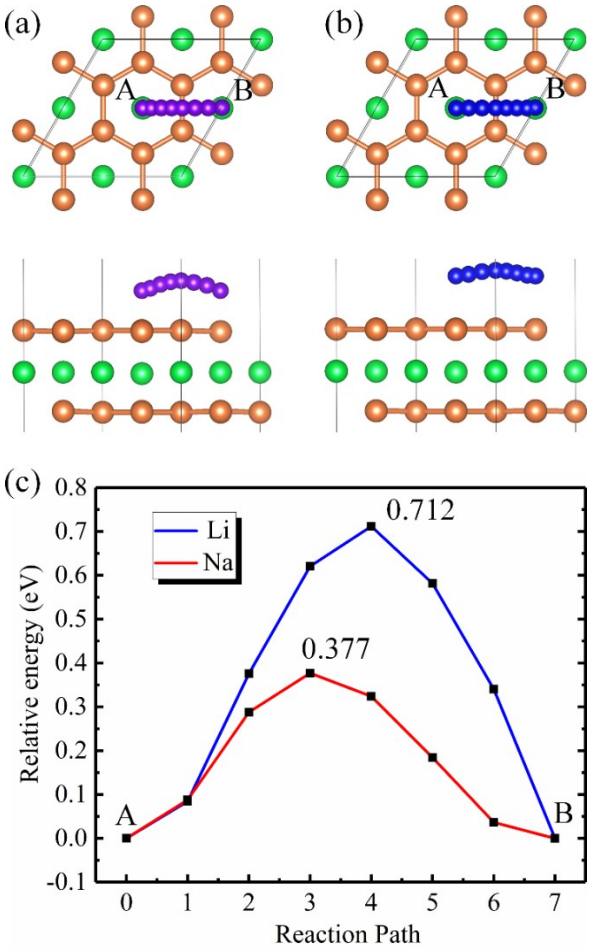

Fig. S13. Top and side views of (a) Li and (b) Na diffusion on the 2D TiB_4 monolayer. (c) Energy profiles of the corresponding Li and Na diffusion pathways. The Ti, B, Li, and Na atoms are denoted by green, orange, violet, and blue spheres, respectively.

6. The intercalation of Li/Na in bilayers of bare Ti_2C, bare Ti_2B_2, $Ti_2B_2H_2$, $Ti_2B_2H_4$, and $Ti_2B_2O_2$.

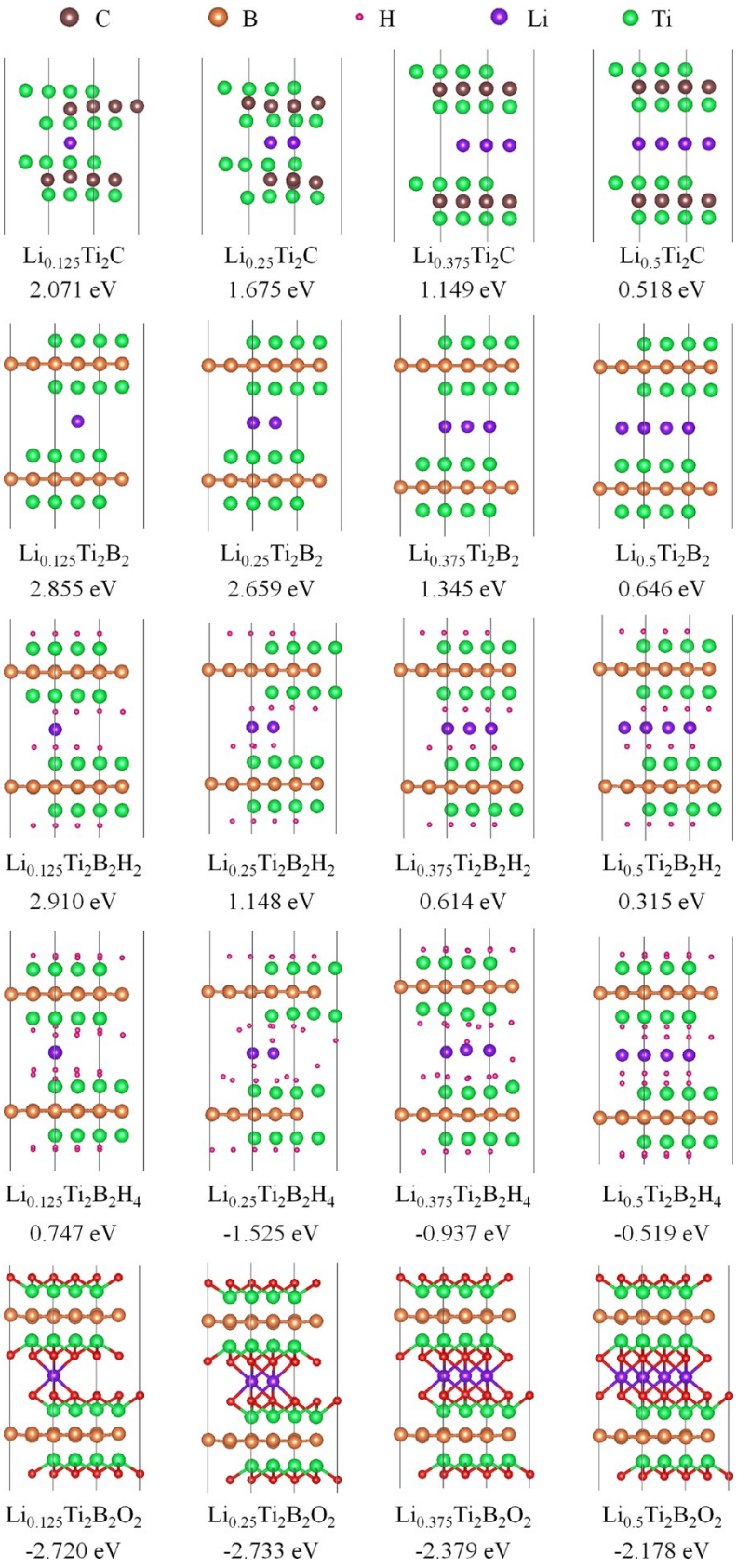

Fig. S14. The optimized structures and intercalation energies for Li intercalation in bilayers of bare Ti_2C, bare Ti_2B_2, $Ti_2B_2H_2$, $Ti_2B_2H_4$, and $Ti_2B_2O_2$.

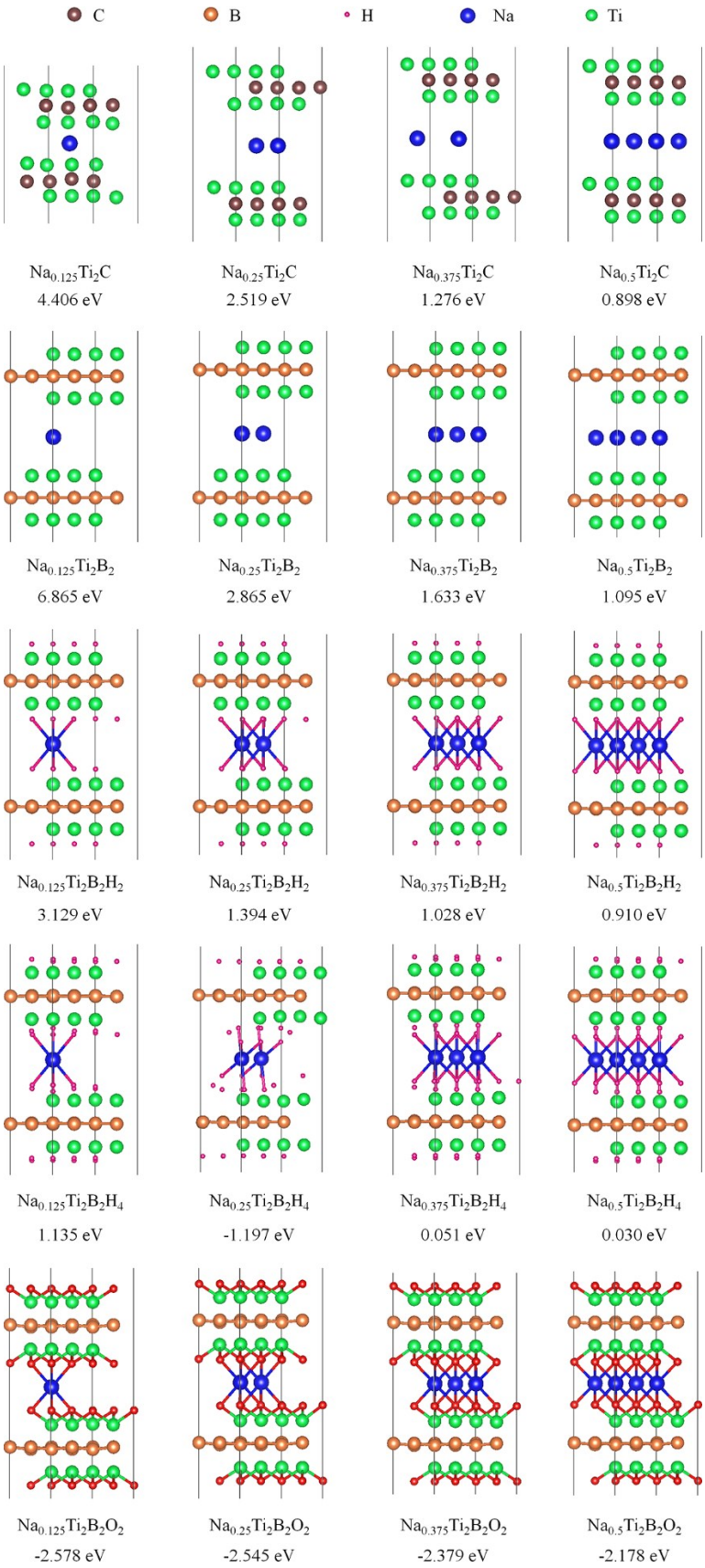

Fig. S15. The optimized structures and intercalation energies for Na intercalation in bilayers of bare Ti_2C, bare Ti_2B_2, $Ti_2B_2H_2$, $Ti_2B_2H_4$, and $Ti_2B_2O_2$.

REFERENCES

1. Y. Wang, J. Lv, L. Zhu and Y. Ma, *Phys. Rev. B*, 2010, **82**, 094116.
2. Y. Wang, M. Miao, J. Lv, L. Zhu, K. Yin, H. Liu and Y. Ma, *J. Chem. Phys.*, 2012, **137**, 224108.
3. Y. Wang, J. Lv, L. Zhu and Y. Ma, *Comput. Phys. Commun.*, 2012, **183**, 2063-2070.
4. G. Kresse and J. Furthmüller, *Phys. Rev. B*, 1996, **54**, 11169-11186.
5. G. Kresse and J. Furthmuller, *Comp. Mater. Sci.*, 1996, **6**, 15-50.
6. G. Kresse and J. Hafner, *Phys. Rev. B*, 1993, **47**, 558-561.
7. J. P. Perdew, K. Burke and M. Ernzerhof, *Phys. Rev. Lett.*, 1996, **77**, 3865-3868.
8. G. Kresse and D. Joubert, *Phys. Rev. B*, 1999, **59**, 1758-1775.
9. P. E. Blöchl, *Phys. Rev. B*, 1994, **50**, 17953-17979.
10. J. Klimeš, D. R. Bowler and A. Michaelides, *Phys. Rev. B*, 2011, **83**, 195131.
11. B. T. Wang and R. M. Elena, *J. Phys. Condens. Mat.*, 2017, **29**, 325501.
12. A. Togo, F. Oba and I. Tanaka, *Phys. Rev. B*, 2008, **78**, 134106.
13. X. Gonze and C. Lee, *Phys. Rev. B*, 1997, **55**, 10355-10368.
14. G. Henkelman and H. Jonsson, *J. Chem. Phys.*, 2000, **113**, 9978-9985.
15. G. Henkelman, B. P. Uberuaga and H. Jonsson, *J. Chem. Phys.*, 2000, **113**, 9901-9904.
16. G. Henkelman and H. Jonsson, *Phys. Rev. Lett.*, 2001, **86**, 664-667.
17. X. Qu, J. Yang, Y. Wang, J. Lv, Z. Chen and Y. Ma, *Nanoscale*, 2017, **9**, 17983-17990.